Proceedings of the Canadian Society for Mechanical Engineering International Congress
32nd Annual Conference of the Computational Fluid Dynamics Society of Canada
Canadian Society of Rheology Symposium
CSME/CFDSC/CSR 2025
May 25–28, 2025, Montréal, Québec, Canada

Characteristics of street canyon flow using Large-Eddy Simulation with a drag-porosity modelled atmospheric boundary layer

Haoran Du[1], Eric Savory[1], Laurent Perret[2]

[1]Department of Mechanical and Materials Engineering, University of Western Ontario, London, Canada
[2]École Centrale de Nantes, CNRS, LHEEA, Nantes Université, Nantes, France
*hdu59@uwo.ca

***Abstract*—**Turbulence and turbulent structures are key features of atmospheric boundary layer flows, playing a crucial role in momentum and energy transport. This study examines the use of a drag-force sink term in the momentum equation, the drag-porosity method, to replicate key characteristics of high Reynolds number boundary layer flows using Large-Eddy Simulation (LES). One-point turbulence statistics are analyzed and compared with previous studies. A street canyon simulation is conducted as a successor simulation, using the boundary layer generated by the drag-porosity method as its inlet condition. Temporally averaged velocity contours reveal the general flow pattern within the street canyon. Overall, the drag-porosity model demonstrates good performance, offering an efficient and low-cost approach for precursor simulations with sufficient accuracy for successive obstacle-resolving LES. More detailed analyses will be presented in the full presentation.

***Keywords-component*—boundary layer; drag porosity; Large-Eddy Simulation; street canyon**

I. INTRODUCTION

Accurately modelling and predicting flow dynamics within urban canopies is essential for understanding street-scale ventilation and scalar dispersion processes, which directly affect pedestrian comfort and air quality. A commonly used approach to studying urban airflow is the street-canyon configuration, which serves as a simplified model for analysing flow characteristics in individual streets or clusters of neighbouring streets. Of particular interest is the case where the upstream flow is perpendicular to the street axis, as this scenario presents the greatest ventilation limitations, leading to reduced pollutant dispersion and increased stagnation zones within the canyon.

Urban canopies form the lowest part of the roughness sublayer within the atmospheric boundary layer and can extend from the ground surface to approximately 2 to 5 times the average canopy height [1]. Turbulence and turbulent structures are key characteristics of atmospheric boundary layer flows, playing a crucial role in momentum and energy transport. The presence of urban roughness significantly influences turbulence generation and modulation, as large-scale atmospheric turbulent structures interact with smaller-scale, canopy-induced structures [2], [3]. Studies have shown that upstream configurations can strongly impact street canyon flows. For example, variations in upstream plan area density [4] or the presence of a tall building [5] can alter the flow dynamics in street canyons. These effects can be attributed to modifications in the oncoming boundary layer caused by upstream urban roughness.

In wind tunnel experiments, spires and fences are placed at the inlet section, followed by cube fetches with the desired plan area density, to generate a fully developed, scaled atmospheric boundary layer. In numerical simulations, precursor simulations, either with or without cyclic boundary conditions between the inlet and outlet, are commonly used to model flow over rough walls, where the roughness geometry is explicitly represented [6]. It is generally believed that geometric roughness must be present to generate turbulence and eddies in wall-modeled Large Eddy Simulation (LES) or Detached Eddy Simulation (DES).

However, the large, dominant eddies observed over rough walls arise from the mean shear but do not rely on specific geometric features [7]. Hence, explicit roughness can be substituted with a drag force that is the same as the force produced by the geometric roughness and, as a result, this drag force disrupts wall streaks in much the same way as geometrical roughness [8]. In urban meteorology studies, the drag-porosity method originated from Reynolds-averaged

Sponsors: The Natural Sciences and Engineering Research Council (NSERC) of Canada and the French National Research Agency (ANR)

Navier–Stokes Simulation (RANS) models, which assumed a constant drag coefficient to characterize the urban canopy [9]. This approach later progressed to LES that incorporate varying drag coefficients depending on height [8], [10], [11]. Although the drag-porosity model does not capture the flow structure within the canopy, because the obstacles are not explicitly represented, it is efficient and low-cost when used as a precursor simulation, for successive obstacle-resolving LES.

II. Methodology

A. Governing equations of the drag-porosity method

The filtered Navier-Stokes equations of the drag-porosity method implemented for LES are written as follow:

$$\frac{\partial \tilde{u}_i}{\partial x_i} = 0 \tag{1}$$

$$\frac{\partial \tilde{u}_i}{\partial t} + \frac{\partial \tilde{u}_j \tilde{u}_i}{\partial x_j} = -\frac{1}{\rho}\frac{\partial \bar{p}}{\partial x_i} + \frac{\partial}{\partial x_j}\left(v\frac{\partial \tilde{u}_i}{\partial x_j} - \tau_{ij}\right) - \frac{F_i}{\rho} \tag{2}$$

where the $\tilde{u}_i$ is the filtered velocity components of the instantaneous streamwise (u_1=U), transverse ($u_2 = V$) and vertical ($u_3 = W$) velocity components, and the sink term F_i/ρ represents the drag effect of the urban canopy in the drag-porosity approach with the drag force term F_i being defined as (3):

$$F_i = \frac{\rho}{2} C_D(z) \alpha_f \tilde{u}_i |\tilde{u}| \tag{3}$$

where ρ is the density of air, $C_D(z)$ is the drag force coefficient profile along the wall-normal direction, α_f is the roughness frontal area per fluid volume which, in a cube fetch with 25% plan area density, is $\alpha_f = 1/(3h)$ with $h = 0.05$m being the scaled average urban canopy height in the present work. $|\bar{u}| = \sqrt{\bar{u}_j \bar{u}_j}$ where u_j is the velocity component in the j^{th} direction.

B. Details of the drag-porosity method based precursor simulation

The drag coefficient coefficient C_D used in the drag-porosity approach can be calculated by the following equation:

$$C_D(z) = \frac{2\Delta p(z)}{\rho U^2(z)} \tag{4}$$

where $\Delta p(z)$ is the mean laterally (y-direction) integrated pressure difference between the front and back faces of a cube and $U(z)$ is the spatially-averaged streamwise mean velocities along the wall-normal direction.

The present work is conducted using OpenFOAM v2406. The one-equation eddy viscosity (kEqn) subgrid-scale (SGS) model is employed for the drag-porosity simulation, with model coefficients $C_e = 1.048$ and $C_k = 0.02654$ is used in the drag-porosity simulation. Spatial derivatives are solved using Gauss linear differencing, while temporal integration is performed using backward differencing. The computational domain measures 4m (streamwise, x) $\times$ 1m (lateral, y) $\times$ 2m (vertical, z). Cyclic boundary conditions are applied at the inlet and outlet (normal to the x-direction) as well as on the front and back boundaries (normal to the y-direction). The top boundary is assigned a slip condition, while the bottom has a no-slip wall condition. The drag porosity zone extends $1.2h = 0.06$m in the z direction from the bottom wall. The meshes are uniform ($\Delta = h/2$) in the x and y directions, as suggested in [8], while it expands in the z-direction with a relative growth ratio of 1.05. The total mesh resolution is 160(x) $\times$ 40(y) $\times$128(z), with 20 cells within the drag-porosity zone in the vertical direction. The simulation is run with a time step of 0.001s. To ensure temporal convergence, the simulation (at the present stage) is first run for an initial period of 50s, followed by an additional 70s over which flow statistics are analyzed.

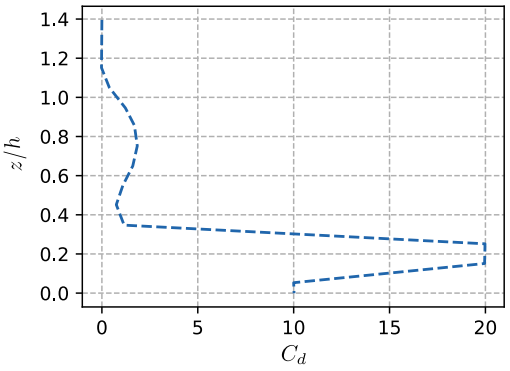

Figure. 1. Vertical profiles of C_d for canopy plan area densities 25% [8].

The outlet patch is recorded at each time step and used as the inlet condition for the successor simulations.

C. Details of the successor simulation of a street canyon

The successor simulation employs the same solver and settings as the precursor simulation. To maintain computational efficiency, the streamwise (x) domain is set to 1m, while the lateral (y) and vertical (z) dimensions remain unchanged at 1m and 2m, respectively. The background mesh resolution is 64(x) $\times$ 64(y) $\times$128(z), with a uniform mesh size. A refined region, which contains the street canyon model, starts from the inlet to $x = 0.65$m, extending from the bottom wall to the height of $z = 0.08$m, with twice finer meshes than the background meshes. Cyclic boundary conditions are applied on the front and back boundaries (normal to the y-direction). The top boundary is treated as symmetric, while the bottom has a no-slip wall condition. The inlet (normal to the x-direction) is prescribed using velocity data from the precursor simulation, while the outlet is treated as a free end with zero pressure.

Fig. 2 shows the configuration of the successor simulation. The street canyon model, represented as two bars with a canyon height-to-width ratio of 1, is placed within a staggered cube array having a 25% plan area packing density. Two rows of cubes are 0.05m downstream of the inlet, and another two rows of staggered cubes are placed 0.05m downstream of the canyon. To reduce computational costs and minimize numerical instabilities that could propagate upstream, poten-

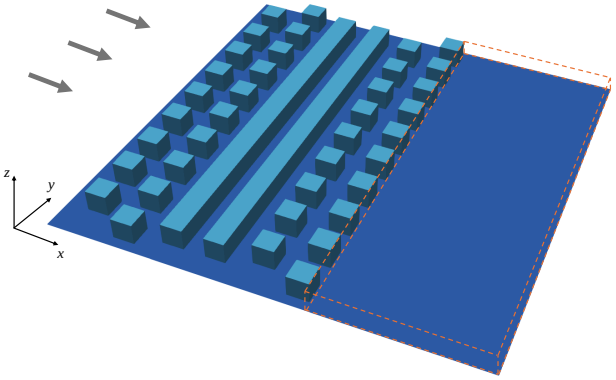

Figure. 2. Schematic of the street canyon model within a staggered cube array with a 25% plan area density. Grey arrows indicate the flow direction, and the dashed orange box represents the drag-porous zone.

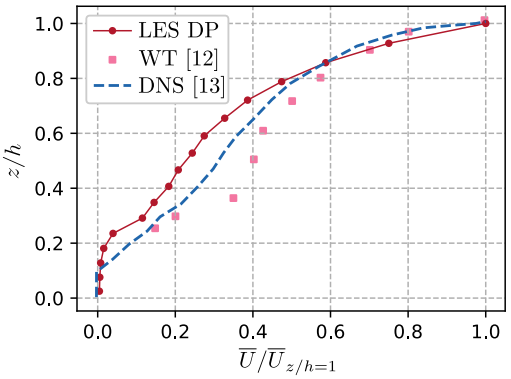

Figure. 3. Vertical profiles of the mean streamwise velocity of the present LES study using the drag-porosity method(LES DP) compared with those of wind-tunnel measurements (WT [12]) and obstacle resolving methods (DNS [13]), normalized by those at the height of $z/h = 1$.

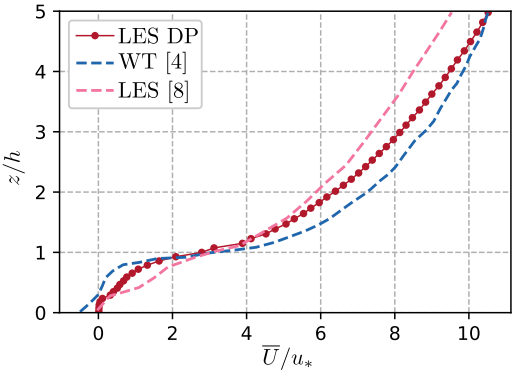

Figure. 4. Vertical profiles of the mean streamwise velocity of the present study (LES DP), normalized by friction velocity,u_*, compared with those of wind tunnel experiments [4] and another drag-porosity method based LES [8].

tially affecting accuracy or causing the simulation to terminate, a drag-porous region is introduced after the last two rows, before the outlet, as shown in the dashed orange box region. This region extends from $x = 0.65$m to the outlet, extending from the bottom wall to the height of $z = 0.08$m. This zone is parameterized using the same urban morphological characteristics as the precursor simulation.

D. Statistics calculation

The instantaneous streamwise (U), transverse (V) and vertical (W) velocity components corresponded to those in the x, y and z directions, respectively. The time-averaged mean streamwise flow velocity is denoted as $\overline{U}$, and the spatially-averaged mean streamwise velocity is denoted as $\langle U \rangle$, which leads to the ensemble averaged streamwise velocity $\langle \overline{U} \rangle$. The Reynolds decomposition in time $U(x,y,z,t) = \overline{U} + u'(x,y,z,t)$ is applied, where $u'(x,y,z,t)$ is the instantaneous velocity fluctuation about the mean $\overline{U}$ (and similarly for the other two directions). The standard deviation of the velocity is defined as $\sigma_u = \sqrt{\overline{(U(x,y,z,t) - \overline{U})^2}}$. The Reynolds shear stress is denoted as $\overline{u'w'} = \overline{(U(x,y,z,t) - \overline{U})(W(x,y,z,t) - \overline{W})}$.

III. Results and Discussions

A. Precursor simulation

The profile in Fig. 3 obtained using the drag coefficient from [8] for a 25% plan area density deviates slightly from the results of [12] and [13], but the overall trend remains consistent. This discrepancy can be attributed to the boundary layer thickness-to-canopy height ratio ($\delta/h \approx 40$) in the present study, which is higher than the ratio of approximately 8 in [12] and [13]. This discrepancy could also be attributed to the applied drag coefficient being too high in the near-wall region, resulting in a reduction in streamwise velocities.

The profile of the temporally averaged streamwise velocity, up to $z/h = 5$ shown in Fig. 4, is scaled by the friction velocity computed from the constant value of Reynolds shear stress $-\langle \overline{u'w'} \rangle$ within a specific height range (discussed later) and compared with results from wind tunnel experiments [4] and another LES study using the drag-porosity method [8]. Within the canopy height, the velocity profile in the present study falls between the LES [8], which exhibits a larger magnitude, and the wind tunnel experiment, which shows a smaller magnitude at the same height. Above the canopy height, the LES profile has a lower magnitude, while the wind tunnel experiment presents a higher magnitude at the same heights. Overall, these findings suggest that the present simulation reasonably captures the wind profile.

The Reynolds shear stress profile, $-\langle \overline{u'w'} \rangle$, along the wall-normal direction is shown in Fig. 5. The friction velocity, u_*, is calculated as 0.15 m/s based on the values of $-\langle \overline{u'w'} \rangle$ within height range of $z/h = 1.2$ to $z/h = 1.5$. The variances of streamwise fluctuations, shown in Fig. 5, are compared with those reported in studies of wind tunnel experiments [4] and another drag-porosity method based LES [8]. Although the values of the variance of the streamwise velocity component observed in the RSL ($1 < z/h < 2$) are consistent with [4], the vertical profiles do not show a good match above. This could be due to the large differences of boundary layer thickness-to-canopy height ratio $\delta/h \approx 20$ in [4].

In Fig. 6, the skewness profile of w' exhibits strong negative

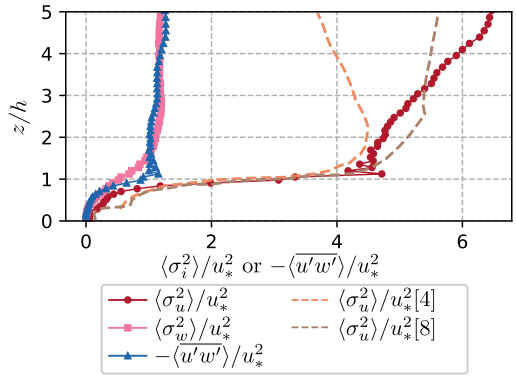

Figure. 5. Vertical profiles of variances of streamwise and vertical components, and Reynolds shear stress $-\overline{\langle u'w'\rangle}$ normalized by u_*^2, compared with the variance of the normalized streamwise components in wind tunnel experiments [4] and another drag-porosity method based LES [8].

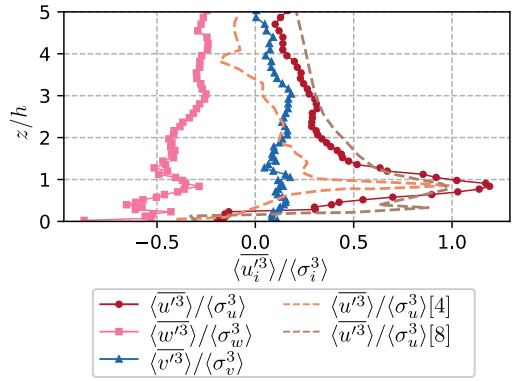

Figure. 6. Vertical profiles of skewness of streamwise, vertical, and transverse components, compared with the skewness of streamwise components in wind tunnel experiments [4] and another drag-porosity method based LES [8].

values within the canopy and the roughness sublayer (RSL). Combined with the strong positive skewness of u' in the RSL, this indicates downward motions in the shear layer. Above the RSL ($z/h > 2$), the streamwise skewness gradually decreases with height, which, in general, shows good agreement with [4] and [8], although in [4], it decreases to negative value at $z/h = 3.2$.

B. Successor simulation

As shown on the right side of Fig. 7, the contours of the temporally averaged streamwise velocity reveals a negative region below $z/h = 0.2$ and a positive region above this height. While this aligns with the general circulation pattern of street canyon flow, the negative regions appear at a lower height compared to the results from wind tunnel experiments [4]. The underlying reason remains to be explored and should be confirmed through further research. Also, the meshes may not fine enough in the near-wall regions.

Fig. 8 displays the contours of the temporally averaged transverse velocity at $z/h = 0.5$. The averaged transverse velocities affect the windward side of the street canyon at the corner, reflecting back to the leeward wall at a lateral distance

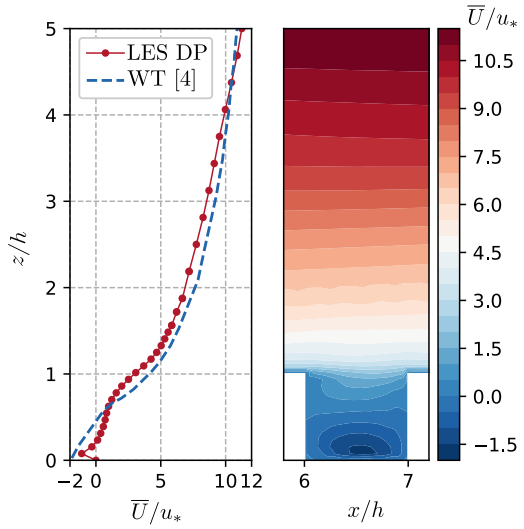

Figure. 7. Left: Normalized vertical profiles of the mean streamwise velocity within the street canyon and the overlying boundary layer (LES DP) at z=0, compared with wind tunnel (WT) results from [4], which used a street canyon with an aspect ratio of 1. Right: Contours of the temporally averaged velocities at $z = 0$ in the present study.

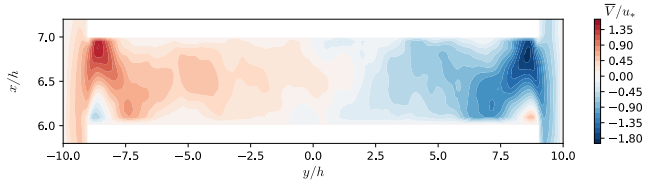

Figure. 8. Contours of the normalized the mean transverse velocity within the street canyon at $z/h = 0.5$.

of 2.5 times the canyon width. The transverse velocities eventually neutralize with the transverse velocity originating from the opposite side.

IV. Conclusions

This article investigates the application of a drag-effect sink term in the LES momentum equation within the region, termed as the drag-porous zone, to generate a boundary layer in the precursor simulation, replicating the boundary layer over a cube fetch. The successor simulation then examines street canyon flow under this fully developed boundary layer.

In the precursor simulation, one-point statistics are compared with wind tunnel experiments and numerical simulations. As expected, the drag-porosity model does not capture the flow structure within the canopy, as the obstacles are not explicitly represented. Overall, the simulated boundary layer shows reasonable agreement with wind tunnel experiments and another boundary layer simulation using the drag-porosity method. However, some discrepancies remain, which can be attributed to differences in the boundary layer thickness-to-canopy height ratios among studies, as well as certain settings in the present study, such as an overly high drag coefficient in the near-bottom regions and insufficient mesh resolution near the wall.

In the successor simulation, the temporally averaged statistics are presented. The general circulation pattern of the street canyon flow is as expected. However, the negative regions appear lower than those observed in wind tunnel experiments, requiring further investigation. The contours of the temporally averaged transverse velocity at $z/h = 0.5$ reveal an unusual finding that the inflow enters the street canyon primarily from the windward side. As it meets the opposing flow from the other side, the transverse flow is neutralized at the centre.

The present work is still under development. Time and grid sensitivity tests will be conducted to ensure the reliability of the simulation. For example, the time history of the cumulative time averages and the skewnesses of the streamwise velocity at specific locations will be analyzed to confirm that the flow has reached a statistically steady state. Additionally, mesh refinement tests will be performed in the successor simulation, including increasing the mesh density by a factor of two and four in the near-wall region, as well as significantly refining the mesh in the shear layer.

In the full presentation, for the precursor simulation of atmospheric boundary layer using drag-porosity method, a comprehensive analysis of one-point turbulence statistics, two-dimensional energy spectra, two-point correlation functions, and the interaction between the most energetic scales will be analyzed and compared with the experiments. For the successor simulation with a long street canyon, a comprehensive analysis of one-point turbulence statistics, integral length scales, and two-point correlations will be compared with previously obtained experimental results, in the wall-normal direction and at the roof level.

The street canyon simulation expands the dataset for street canyon studies and serves as a crucial step toward the development of reduced-order models.

ACKNOWLEDGMENT

The authors thank the Natural Sciences and Engineering Research Council (NSERC) of Canada and the French National Research Agency (ANR) for providing funding.

REFERENCES

[1] J. C. Kaimal and J. J. Finnigan, Atmospheric Boundary Layer Flows: Their Structure and Measurement. NY, NY: Oxford University Press, 2020.

[2] K. Blackman, L. Perret, and E. Savory, "Effects of the upstream-flow regime and canyon aspect ratio on non-linear interactions between a street-canyon flow and the overlying boundary layer," Boundary-Layer Meteorology, vol. 169, no. 3, pp. 537–558, Jul. 2018. (*doi:10.1007/s10546-018-0378-y*)

[3] H. Du, L. Perret, and E. Savory, "Effect of urban morphology and an upstream tall building on the scale interaction between the overlying boundary layer and a street canyon," Boundary-Layer Meteorology, vol. 190, no. 2, Jan. 2024. (*doi:10.1007/s10546-023-00844-8*)

[4] K. Blackman, L. Perret, and E. Savory, "Effect of upstream flow regime on street canyon flow mean turbulence statistics," Environmental Fluid Mechanics, vol. 15, no. 4, pp. 823–849, Oct. 2014. (*doi:10.1007/s10652-014-9386-8*)

[5] H. Du, E. Savory, and L. Perret, "Effect of morphology and an upstream tall building on the mean turbulence statistics of a street canyon flow," Building and Environment, vol. 241, p. 110428, Aug. 2023. (*doi:10.1016/j.buildenv.2023.110428*)

[6] U. Shaukat and K. E. T. Giljarhus, "Precursor turbulent inflow dataset for large eddy simulation of a semi-idealized European generic city," Data in Brief, vol. 54, p. 110467, Apr. 2024. (*doi:10.1016/j.dib.2024.110467*)

[7] J. Varghese and P. A. Durbin, "Representing surface roughness in eddy resolving simulation," Journal of Fluid Mechanics, vol. 897, Jun. 2020. (*doi:10.1017/jfm.2020.368*)

[8] Q. Bucquet, I. Calmet, L. Perret, and M. Maché, "Large-eddy simulation of the urban boundary layer using drag-porosity modeling," Journal of Wind Engineering and Industrial Aerodynamics, vol. 238, Apr. 2023. (*doi:10.1016/j.jweia.2023.105432*)

[9] O. Coceal and S. E. Belcher, "A canopy model of mean winds through urban areas," Quarterly Journal of the Royal Meteorological Society, vol. 130, no. 599, pp. 1349–1372, Apr. 2004. (*doi:10.1256/qj.03.40*)

[10] G. Tian, "Analysis of the unsteady boundary-layer flow over urban-like canopy using large eddy simulation," Theses, École centrale de Nantes, 2018. [Online]. Available: https://theses.hal.science/tel-02096983

[11] E. J. Bannister, X. Cai, J. Zhong, and A. R. MacKenzie, "Neighbourhood-Scale flow regimes and pollution transport in cities," Boundary-Layer Meteorology, vol. 179, no. 2, pp. 259–289, Dec. 2020. (*doi:10.1007/s10546-020-00593-y*)

[12] I. P. Castro, H. Cheng, and R. Reynolds, "Turbulence over urban-type roughness: Deductions from wind-tunnel measurements," Boundary-Layer Meteorology, vol. 118, no. 1, pp. 109–131, Jan. 2006. (*doi:10.1007/s10546-005-5747-7*)

[13] S. Leonardi and I. P. Castro, "Channel flow over large cube roughness: A direct numerical simulation study," Journal of Fluid Mechanics, vol. 651, pp. 519–539, Apr. 2010. (*doi:10.1017/s002211200999423x*)